

B-spline parameterization of spatial response in a monolithic scintillation camera

V. Solovov*, A. Morozov, V. Chepel, V. Domingos, R. Martins

*LIP-Coimbra and Department of Physics of the University of Coimbra,
3004-516 Coimbra, Portugal*

E-mail: solovov@coimbra.lip.pt

ABSTRACT: A framework for parameterization of the light response functions (LRFs) in a scintillation camera was developed. It is based on approximation of the measured or simulated photosensor response with weighted sums of uniform cubic B-splines or their tensor products. The LRFs represented in this way are smooth, computationally inexpensive to evaluate and require much less memory than non-parametric alternatives. The parameters are found in a straightforward way by the linear least squares method. The use of linear fit makes the fitting process stable and predictable enough to be used in non-supervised mode. Several techniques that allow to reduce the storage and processing power requirements were developed. A software library for fitting simulated and measured light response with spline functions was developed and integrated into an open source software package ANTS2 designed for simulation and data processing for Anger camera-type detectors.

KEYWORDS: Scintillation detectors; Data processing methods; Simulation methods and programs.

*Corresponding author.

Contents

1. Introduction	1
2. B-Splines	3
2.1 Uniform cubic B-splines	3
2.2 Tensor product splines	4
3. LRF parameterization	4
3.1 Use of axial symmetry	5
3.2 Compressed axial LRFs	6
3.3 General 2D LRFs	7
3.4 Array symmetry and sensor groups	7
4. Implementation details	8
4.1 Fitting of the data	8
4.2 Storage and evaluation	9
5. Examples	9
6. Conclusions	11
7. Acknowledgment	12

1. Introduction

Scintillation camera, first developed by H. Anger more than 50 years ago [1], remains an effective tool in areas as diverse as medical imaging [2], astrophysics [3] and neutron detection [4]. Since the invention of the camera and until now the Center of Gravity (CoG) algorithm remains the most widely used method for position reconstruction of scintillation events. Its simplicity, and the fact that it can be implemented using analog circuitry makes it the method of choice despite several drawbacks, the most notable of which is distortion of the reconstructed image especially severe at the periphery of the scintillator crystal. In modern commercial devices this distortion is corrected typically by means of a look-up table [5]. However, the peripheral part of the crystal is not used as the image quality there remains poor even after correction. Also, maintaining high image quality in the used area requires frequent detector re-calibrations, considerably increasing the running costs.

An alternative approach is to use statistical position reconstruction techniques [6], [7] (e.g. based on maximum likelihood or least squares methods), that reconstruct an event by finding its parameters (typically, position and energy) for which the predicted detector response is in the best

agreement with the observed one. These techniques can produce distortion-free image and also permit filtering of the noise events such as, for example, multiple gamma ray scatter or electromagnetic interference. On the other hand, these techniques are much more demanding in terms of the processing power and require a detailed characterization of the response of the light sensor array to scintillation light for accurate reconstruction.

Recently, due to widespread use of parallel processing hardware, both in the form of multi-core processors and graphics processing units (GPU), it becomes possible to run real-time position reconstruction using statistical algorithms on a consumer-grade personal computer. As for the sensor array calibration, it can be performed automatically, for example, using a collimated gamma source mounted on a coordinate table controlled by a computer. Also, recently an iterative algorithm for reconstructing the detector spatial response from uniform gamma-ray irradiation data was developed for ZEPLIN III dark matter detector [8]. Later, it was successfully applied to the analysis of experimental data from several radiation detectors with optical readout similar to that used in Anger camera: LUX liquid xenon dark matter detector [9], thermal neutron position-sensitive detectors [10], as well as to a medical gamma camera [11].

When developing software tools for statistical reconstruction, one is faced with the problem of storage of the detector response model. It can be stored either in non-parametric form, for example, as a look-up table, or can be parameterized as a set of light response functions (LRFs) that characterize the response of individual photosensors as functions of coordinates. The second approach has several advantages:

- the reduced storage requirements, which is especially important for processing on GPUs where the amount of fast memory is limited
- the parameterization can be also used as a regularization technique constraining the LRF to the required degree of smoothness, or ensuring it's symmetry or monotonicity. This regularization is particularly important for improving stability of the iterative response reconstruction [11]
- smooth dependence on coordinates improves efficiency of minimization algorithms used for position reconstruction

Analytic representation, the most widely used parameterization scheme, is more robust than others as it typically uses fewer parameters and is based on a physical detector model. However, adequate analytic representation is geometry-specific and can be difficult to find. This makes it less suitable for a generic software package that is expected to work with detectors of various geometries. Alternatively, cubic spline representation, proposed in [12] and also used in [8], is flexible enough to handle arbitrary detector configuration while preserving all the advantages of the parametric approach.

Our group has built a comprehensive set of software tools for scintillation cameras, including simulation, detector response reconstruction, data processing, event reconstruction and analysis, distributed as an open source software package ANTS2 [15]. This required to develop a technique to store the detector response model that at the same time (i) have moderate storage requirements, (ii) permit fast evaluation, (iii) can be used with detectors of arbitrary geometry and (iv) be robust

enough to be used in unsupervised mode. Cubic spline parameterization, widely used in engineering applications for interpolation and data smoothing, was found to satisfy all the criteria listed above. The software library was developed for fitting photosensor response with splines in two dimensions. Also, several techniques of reducing the total number of parameters by taking into account the spatial symmetry of photosensor response were designed. The implementation details and a few application examples are presented in this paper.

2. B-Splines

The splines in general are a class of piecewise polynomial functions with continuous derivatives up to a certain degree. The splines made of higher degree polynomials are smoother but more costly to evaluate. We have decided to use cubic spline for LRF parameterization as it guarantees the smooth first derivative (important for convergence of several minimization algorithms) while still not being too computationally expensive.

2.1 Uniform cubic B-splines

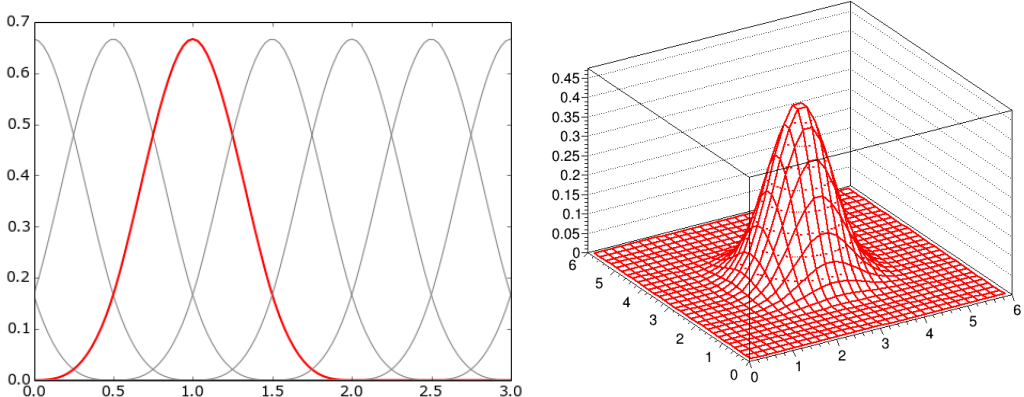


Figure 1. An example of the full basis formed by uniform cubic B-splines on the segment $[0, 3]$ (left). Two dimensional tensor product of two UCBS (right). The labels on the horizontal axes coincide with the knot positions.

The B-splines (basis splines) are a set of functions, which form a basis for the spline functions of a given degree over a certain interval $[x_0, x_1]$, i.e. any spline can be represented as a linear combination of B-splines:

$$S(x) = \sum_k w_k B_k(x) \quad (2.1)$$

where $B_k(x)$ are the B-splines and w_k are the spline coefficients. Each B-spline of n -th degree consists of $n+1$ polynomial segments separated by control points called knots. The shape of a B-spline is defined by its degree and the placement of the knots. In the case of uniform B-splines the knots are spaced with equal intervals and all $B_k(x)$ are shifted copies of each other:

$$B_{k+1}(x) = B_k(x - d) \quad (2.2)$$

or, equivalently:

$$B_k(x) = B_1(x - (k - 1)d), \quad (2.3)$$

where d is the interval between the knots. In the case of uniform cubic B-splines (UCBS), B-spline consists of four cubic segments arranged to ensure continuity of the second derivative as shown by the thick red curve in left plot of Figure 1 which also shows an example of the full basis made of B-splines for a segment (in this case $[0, 3]$). Please refer to [13] and [14] for detailed description of B-splines and their properties.

While non-uniform splines offer greater flexibility they require additional storage for the knot positions. They are more expensive to evaluate as well because before computing the polynomial the corresponding segment must be found using binary search. For these reasons, it was decided to base the LRF parameterization on the UCBS.

2.2 Tensor product splines

B-spline representation can be expanded to two or more dimensions using tensor products. For example, in the 2D case one can write, similarly to 2.1:

$$S(x, y) = \sum_k \sum_l w_{kl} B_k(x) B_l(y) \quad (2.4)$$

Here $B_k(x) B_l(y)$ is a product of one-dimensional B-splines in x and y directions. A single two-dimensional tensor product of UCBS is shown on the Figure 1 (right). It consists of 16 bi-cubic segments and retains attractive features of one-dimensional B-splines, such as smoothness of the first derivatives and compact support.

3. LRF parameterization

LRF characterizes spatial dependence of response of a given photo sensor in a scintillation camera. It can be defined everywhere inside the scintillator volume and in the general case is a function of three coordinates. However, in many practical applications the scintillator is thin enough to disregard the dependence of the LRFs on the depth of interaction z and consider them to depend on x and y only. We will assume that this is the case for the rest of the discussion.

Typically, an event in a scintillation camera (a gamma-ray interacting with the scintillator) is recorded as a vector of signal amplitudes registered by the photosensor array. In the following discussion, only events resulting in a single scintillation point will be considered. For an event producing in total N isotropically emitted photons, due to statistical nature of photon detection, each element of this vector is a random number distributed with expectation value of

$$\langle A_i \rangle = N C_i \eta_i(x, y), \quad (3.1)$$

where A_i is the signal amplitude, η_i is the LRF and C_i is scaling factor (gain), all for i -th photosensor. The gains C_i become important when using the same LRF parameterization for several photosensors as described in section 3.4. To find the LRF, one needs a set of data points each

containing photosensor response, the event coordinates and the number of emitted photons. The function 3.1 is fitted to this dataset to obtain the LRF parameters that most closely describe the available data as shown in Figure 2.

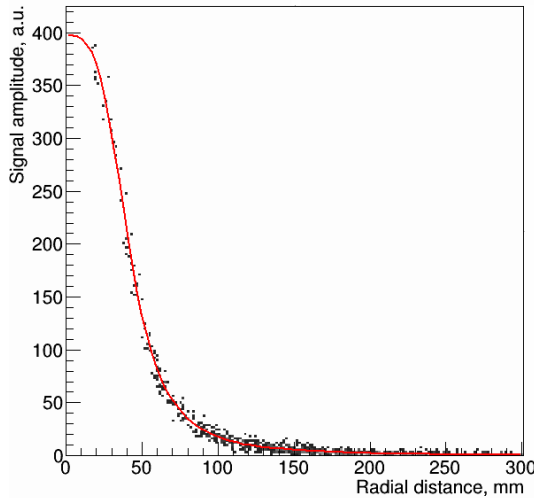


Figure 2. Example of parametrization of axially symmetric response of a photosensor (PMT in a medical gamma camera). The points show signal amplitude of one of the PMTs plotted against the distance from the simulated event positions to the axis of the PMT. The line is the fit of the points with a cubic spline.

Well implemented parameterization should satisfy the following criteria:

- (a) faithful representation of the LRF. The deviations from the true function will create bias in the reconstructed position which in turn will lead to distortions in the reconstructed image. The tolerance to such deviations depends on the application but as a rule of thumb one can assume that the deviations can be considered acceptable if they are significantly smaller than statistical fluctuations of the photosensor signals;
- (b) optimal number of parameters, i.e. the minimum number of parameters that is required to satisfy property (a). Minimizing the parameter count, besides reducing the storage requirements, also leads to less data points required for the fit, less susceptibility to overfitting and faster fit as well;
- (c) stable unsupervised fitting. This is important for use in a software package, especially in unsupervised mode. For this reason, linear least squares is the preferable method for performing the fit.
- (d) fast evaluation. The LRF evaluation is the most often called routine (typically ranging from hundreds to thousands times) for each reconstructed event, so its efficiency directly influences the time required for reconstruction.

3.1 Use of axial symmetry

Generally, an LRF must be fitted by a function of two variables (Equation 2.4) to correctly represent its shape. However, in many cases the dimensionality of representation can be reduced. If one

assumes the response of a photosensor to be axially symmetric, this makes it a function of only one variable r , which is the distance from the photosensor axis. In this case the LRF can be represented with a spline (Equation 2.1) as a function of r :

$$\eta(x, y) = \sum_k w_k B_k(r) = \sum_k w_k B_k(\sqrt{(x - X_0)^2 + (y - Y_0)^2}), \quad (3.2)$$

where $\eta(x, y)$ is the LRF and X_0 and Y_0 are the coordinates of the photosensor axis.

The use of axially symmetric LRFs, when applicable, permits to significantly reduce the required number of parameters and speed up LRF evaluation. Also, in the case of iterative reconstruction of the LRFs from the flood data, the axial symmetry provides sufficient regularization to ensure convergence even at low photon statistics [11].

The most straightforward case for use of axially symmetric LRFs is a photomultiplier tube (PMT) with a circular photocathode. It can also be applied to hexagonal and even square photosensors, provided the lightguide thickness is comparable with the sensor size, as demonstrated in section 5.

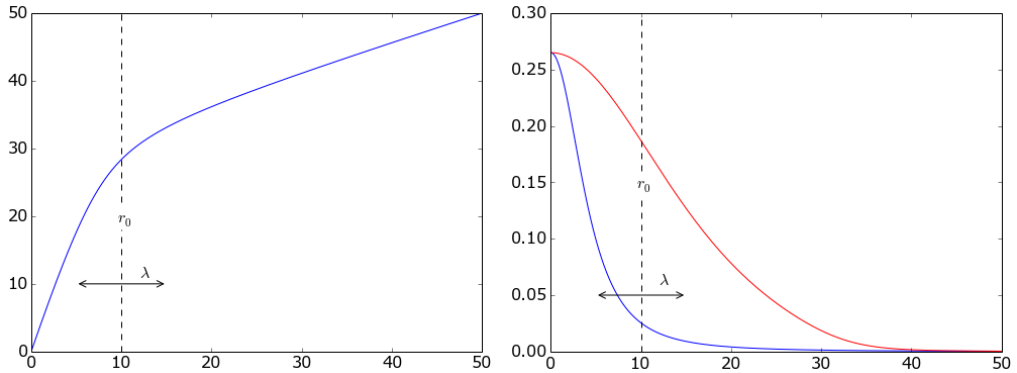


Figure 3. Left: nonlinear scale transformation from r to ρ ; right: the same LRF shown as a function of r (blue curve) and ρ (red curve).

3.2 Compressed axial LRFs

Typically, an LRF $\eta(x, y)$ exhibits non-uniform variation rate: it rapidly grows as the argument (x, y) approaches the corresponding photosensor. This results in a conflict when optimizing the number of knots for a uniform spline: on one hand, the inter-knot distance must be sufficiently short to faithfully represent the region of rapid function change, on the other hand, this leads to too many knots covering the slowly changing region. Consequently, for a large photosensor array most of the spline storage is used with little efficiency. Moreover, excessive number of knots may be the cause of LRF overfitting and subsequent artifacts in event reconstruction. An obvious solution to this problem would be the use of non-uniform splines, however, the associated memory and computational overheads were considered prohibitive.

An alternative solution was implemented for axially-symmetric LRFs $\eta(r)$ in our parameterization library. A new variable $\rho(r)$ is introduced

$$\rho = a \left(\frac{\kappa + 1}{\kappa - 1} (r - r_0) - \sqrt{(r - r_0)^2 + \lambda^2} + b \right) \quad (3.3)$$

that depends on r and varies faster for smaller r (closer to the photosensor) and slower for larger r . The ratio between the variation rates at the origin and at infinity is defined by the constant κ , while r_0 and λ define the center point and smoothness of transition between the two (Figure 3, left). Constants a and b are chosen to ensure that ρ covers the same domain as r . An LRF $\eta(\rho)$, as a function of this new variable, has its part close to the origin stretched and at large distances compressed as shown in Figure 3, right. After such transformation, $\eta(\rho)$ requires less knots (and less memory) than the original $\eta(r)$ to achieve the fit (as a weighted sum of UCBS) of the same precision. The particular function 3.3 was chosen because the user-defined parameters κ , r_0 and λ are easy to choose empirically from the observed shape of $\eta(r)$, while a and b are computed automatically.

3.3 General 2D LRFs

There are detector configurations where the light response is not symmetric at least for some of the photosensors. One example is a sensor close to the side boundary of the crystal of a compact gamma camera shown in Figure 5. For such cases, the LRF must be fitted by a function of two variables (see Eq. 2.4) to correctly represent its shape. The number of knots in both directions should be carefully optimized as the parameter count grows proportionally to the product of the number of knots which in turn results in rapid increase in the storage requirements and in the time necessary for fitting.

3.4 Array symmetry and sensor groups

It is possible to take advantage of the symmetry of the photosensor array geometry and use common LRF parameterization for several sensors. This is done by arranging the sensors into the groups so that the same LRF can be used for all sensors in the group, after proper coordinate transform consisting of combination of rotation, translation and reflection. Such approach not only reduces the storage requirements but also effectively multiplies the number of events, available for LRF fitting, by the number of the sensors in the group. To account for the differences in the individual channel sensitivity, the gain parameter C_i is assigned to each sensor in the group. To calculate the expected response the common group LRF is scaled with this gain parameter according to equation 3.1.

In the extreme case of such grouping, a single axial LRF for all photosensors can be used. Despite the simplicity, it works well for the geometries where the fraction of reflected light is negligible [8]. It was also found useful for the iterative LRF reconstruction in a medical gamma camera [11]. There it was used for the first few iterations before switching to iterations with individual LRFs to refine the result.

More complex grouping can be done using rotational or reflection symmetry of the photosensor array. This allows to arrange the sensors in groups of 2 and 4 for a rectangular array, groups of 4

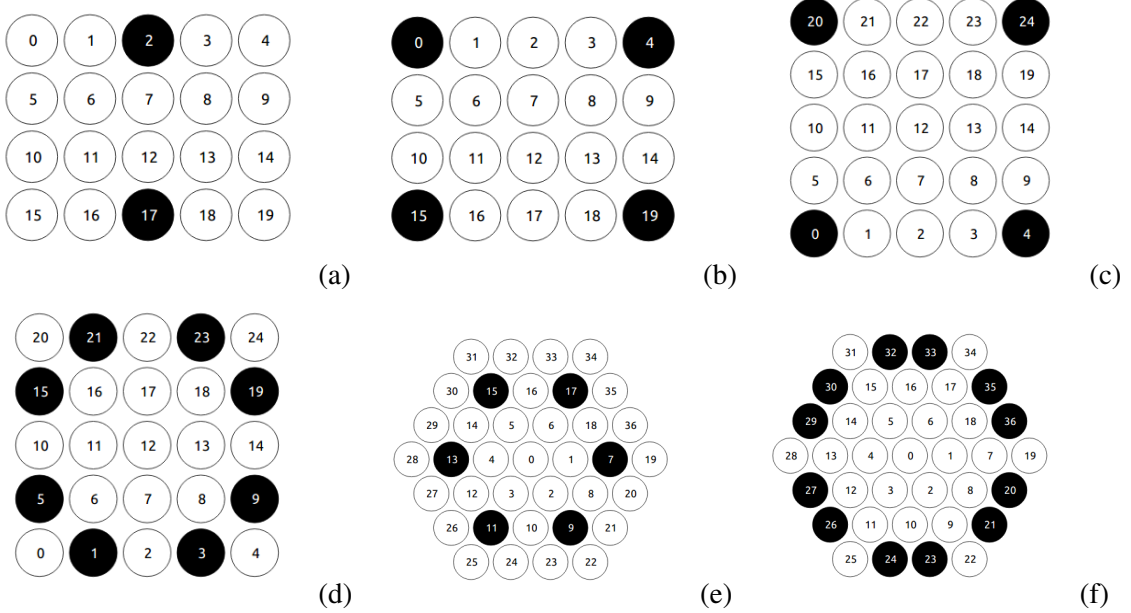


Figure 4. Examples of groups based on rotational and reflective symmetry in rectangular (a, b), square (c, d) and hexagonal (e, f) arrays of photosensors.

and 8 for a square array and groups of 6 and 12 for a hexagonal one as shown in Figure 4. For cameras with rotational symmetry, another method can also be used which is grouping photosensors according to their distance from the camera axis.

4. Implementation details

4.1 Fitting of the data

The spline coefficients w_k are computed using linear least squares fit to the experimental or simulated dataset made of records containing photosensor response, the event coordinates and the number of emitted photons (estimated in the case of experimental data). To make the fitting more efficient, the data points are binned (it is technically possible to make fit through the all the data points but the time required for the fit becomes impractical for datasets of more than a few thousand points). The binning is done by radius from the photosensor for axial LRFs or by (x, y) position otherwise. Our library uses 4 bins per spline interval which proved to be adequate for the detector geometries we used so far. The w_k are then found by solving over-determined system of linear equations $\sum_k B_{kj} w_k = z_j$ where B_{kj} is the value of k -th B-spline in the middle of j -th bin and z_j is the photosensor response averaged over all the points that fall into the j -th bin. In the case of axially-symmetric LRF extra equations are added to force derivative at the origin to be zero. Depending on the user's choice, the solution can be found by either QR-decomposition or singular value decomposition (SVD). However, even when more robust SVD is used, the fitting is not particularly tolerant to the presence of empty bins so care should be taken to make sure that the whole scintillator area is represented by the data points.

When the photosensors are grouped as described in 3.4 a single LRF is fitted for all photosensors in a group. In this case each of the data points is "cloned" using the same coordinate transform that is applied to calculate LRF of the group members, effectively multiplying the number of points available for the fit by the number of photosensors in the group.

4.2 Storage and evaluation

The fitted spline can be stored in two formats, depending on the intended usage. Storing it as a set of coefficients w_k is most efficient in terms of memory usage, requiring $n + 3$ variables per LRF, where n is the number of intervals. However, this format is more computationally expensive as an LRF must be found as a sum of 4 cubic polynomials in this case. Alternative approach, based on the fact that a spline itself is a piecewise polynomial, is to pre-compute and store polynomial coefficients for each interval. In this case only one cubic polynomial have to be computed but $4n$ values must be stored per LRF. These differences are even more pronounced for the tensor product splines. In the ANTS2 package, the first method is used for reconstruction on GPU where the amount of fast memory is limited and the second for reconstruction on CPU where storage is not a limiting factor.

5. Examples

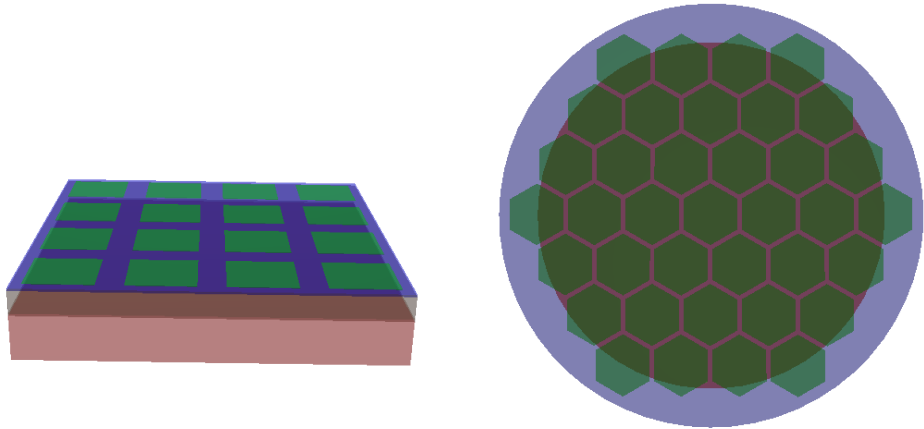


Figure 5. Gamma camera models used as the examples: a compact camera with LYSO crystal and SiPM readout (left) and a gamma camera of standard configuration with NaI(Tl) crystal and PMT readout (right).

In this section we demonstrate viability of the technique described above on two simulated examples. The first of these examples deals with event reconstruction in a compact scintillation camera shown in Figure 5 (left). It consists of a $16 \times 16 \times 2$ mm³ LYSO scintillator crystal (pink) coupled to an 4×4 array of 3×3 mm² silicon photomultipliers (SiPMs) (green) through a 1.5 mm

thick light guide (blue). The SiPM array is modeled after SensL ArrayC-30035-16P-PCB array [16], including dimension, photon detection efficiency, noise and micro-cell count. The simulations and reconstructions were performed using ANTS2 package. Each scintillation event was simulated by isotropic emission of a given number of optical photons at a random position inside the scintillator and performing 3D ray tracing considering the optical properties of the materials and their interfaces. The obtained photosensor signals were used to calculate the spline coefficients of a chosen parameterization scheme. The obtained LRFs, in turn, were used to reconstruct the event positions applying the method of maximum likelihood. To assess performance of the reconstruction, scintillation events were simulated on a square grid inside the crystal with 100 events per grid node and the density maps of reconstructed positions were analyzed.

The reconstructed positions from the events simulated on a 2×2 mm grid are shown in Figure 6. The left image was obtained using axially symmetric functions to parametrize the LRFs of the SiPMs in the detector. While this approach may seem counter-intuitive due to square shape of the SiPMs, it works very well for the internal part of the camera. The reconstruction only fails near the border of the crystal, where the reflections from the side walls break axial symmetry of the light response. The image on the right was obtained using general 2D LRF parameterization with 15 spline intervals in each direction. As one can see, there is notable improvement in the border region while the internal part is essentially identical to that in the left image made with axially symmetric LRFs.

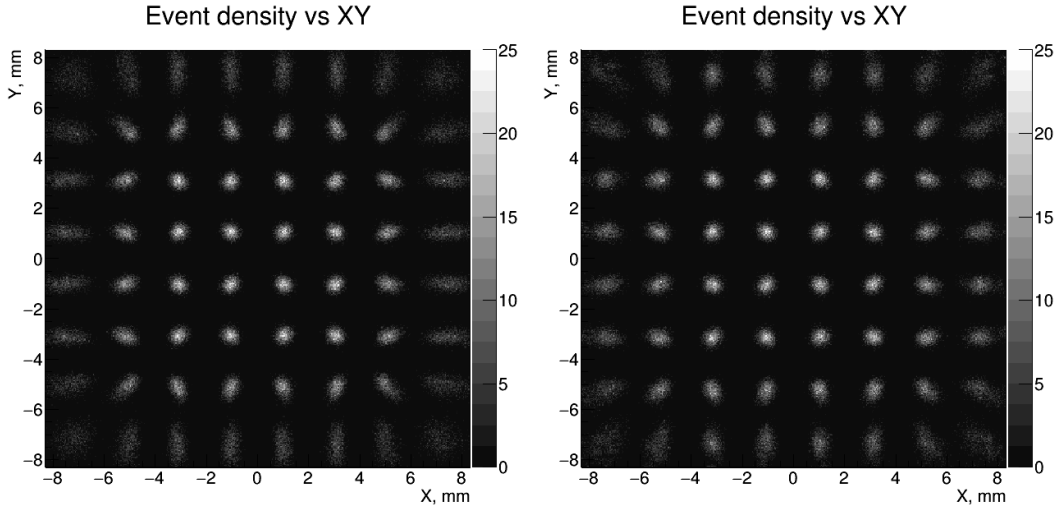


Figure 6. Density maps of reconstructed positions of the events simulated on a square grid with 2 mm pitch for axially symmetric (left) and 2D (right) LRFs.

The second example demonstrates how the quality of reconstructed image in a medical gamma camera can depend on the choice of LRF parameters, namely the number of spline intervals and the use of compression. It is based on the model of the camera used to investigate iterative LRF reconstruction. This camera consists of a $\phi 470$ mm NaI(Tl) scintillator crystal and a $\phi 570$ mm glass lightguide, both 12.5 mm thick. The readout is done by an array of 37 hexagonal PMT coupled to the lightguide (see Figure 5 (right)). In this case, simulation included irradiation of the camera with

a collimated beam of 140 keV γ -rays followed by propagation of scintillation photons. The flood data, obtained by uniform camera irradiation, were used to fit the LRFs. To obtain the test data (used for the assessment of reconstruction quality) a mask made of 10 mm wide and 3mm thick lead bars was placed in the beam path in front of the camera. The further details on the gamma camera geometry and simulation parameters can be found in [11].

The images of the mask reconstructed using axial LRF parameterization are shown in Figure 7 for (from left to right) 8, 12 and 16 intervals per spline. The top row of images was obtained using uniform splines without compression while for the images in the bottom row the radius transformation 3.3 was employed. As one can see, use of compression results in a considerably less distorted image for an equal number of intervals. In fact, compressed 8-interval and not compressed 16-interval representations yield reconstructed images with similar degree of distortion.

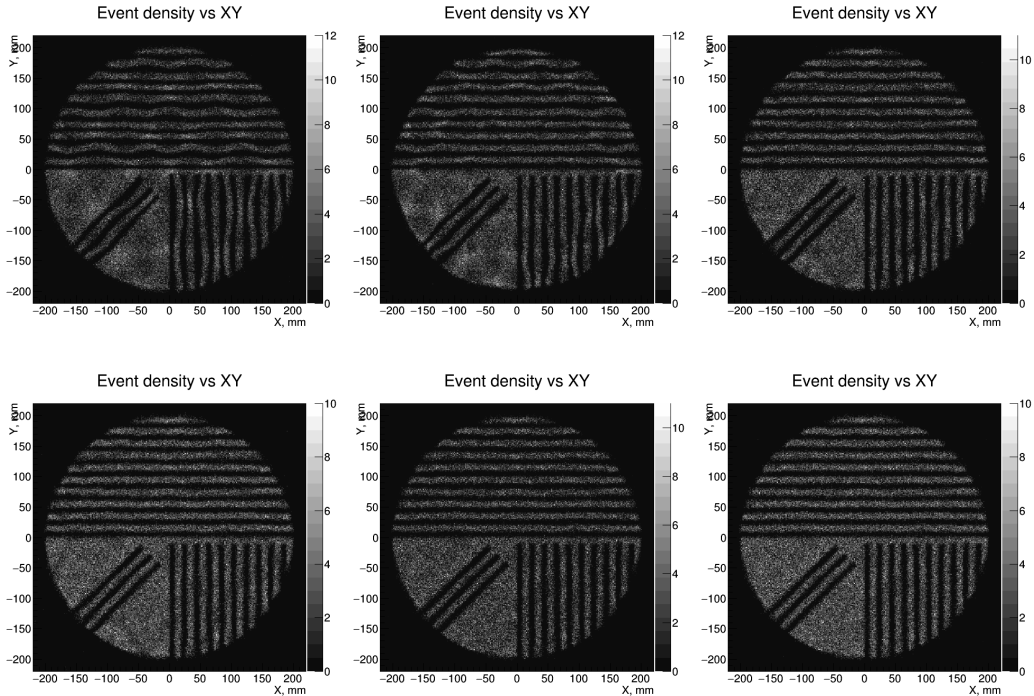


Figure 7. Mask image reconstructed using axial LRF parameterization with 8 (left), 12 (middle) and 16 (right) intervals per spline. Top row: no compression, bottom row: compression with $\kappa = 5$, $r_0 = 150\text{mm}$ and $\lambda = 50\text{mm}$.

6. Conclusions

A framework was developed for parameterization of the light response functions of photosensors in a scintillation camera. It is based on approximation of the measured or simulated photosensor response with weighted sums of uniform cubic B-splines or their tensor products. The LRFs parameterized in this way are smooth, computationally inexpensive to evaluate and typically require much less storage than non-parametric alternatives. The parameters are found in a straightfor-

ward way by the linear least squares method which is stable and predictable enough to be used in non-supervised mode.

Both the axial symmetry of the photosensor response and symmetry of the photosensor array can be exploited in the framework to improve stability of the parameterization and reduce the storage requirements. An optional non-linear coordinate transform permits to further reduce the required storage while maintaining faithfulness of parameterization. It can also be used as an additional LRF regularization tool allowing to avoid overfitting.

The framework is implemented in an open source software package ANTS2 designed for simulation and experimental data processing for Anger camera-type detectors. Examples of the framework application are demonstrated for two broadly used types of scintillation camera geometries.

7. Acknowledgment

This work was carried out with financial support from Fundação para a Ciência e Tecnologia (FCT) through the project-grant PTDC/BBB-BMD/2395/2012 (co-financed with FEDER/COMPETE) and grant IF/00378/2013/CP1172/CT0001 as well as from Quadro de Referência Estratégica Nacional (QREN) in the framework of the project Rad4Life.

References

- [1] H. O. Anger, *Scintillation camera*, *Review of Sci. Instr.* **29** (1958) 27.
- [2] J. T. Bushberg, J. A. Seibert, E. M. L. Jr, and J. M. Boone, *The Essential Physics of Medical Imaging, Third Edition*. LWW, Philadelphia, third, north american edition edition ed., Dec., 2011.
- [3] W. Cook, M. Finger, and T. Prince, *A thick anger camera for gamma-ray astronomy*, *IEEE Trans. on Nuc. Sci.* **32** (1985), no. 1 129–133.
- [4] J. Schelten, R. Engels, and R. Reinartz, *Maximum-likelihood principle for determining positions in neutron scintillation detectors*, *IEEE Trans. on Nuc. Sci.* **47** (2000) 2699–2705.
- [5] T. E. Peterson and L. R. Furenlid, *SPECT detectors: the Anger Camera and beyond*, *Phys. Med. Biol.*, **56** (2011) R145.
- [6] H. H. Barrett, W. C. J. Hunter, B. W. Miller, S. K. Moore, Y. Chen, and L. Furenlid *Maximum-Likelihood Methods for Processing Signals From Gamma-Ray Detectors*, *IEEE Trans. on Nuc. Sci.* **56** (2009), no. 3, Part 2 725–735.
- [7] J. Hesterman, L. Caucci, M. Kupinski, H. Barrett, and L. Furenlid, *Maximum-likelihood estimation with a contracting-grid search algorithm*, *IEEE Trans. on Nuc. Sci.* **57** (2010) 1077–1084.
- [8] V. N. Solovov, V. A. Belov, D. Y. Akimov, H. M. Araujo, E. J. Barnes, A. A. Burenkov et al., *Position reconstruction in a dual phase xenon scintillation detector*, *IEEE Trans. on Nuc. Sci.* **59** (2012) 3286 –3293.

- [9] D. S. Akerib, X. Bai, E. Bernard, A. Bernstein, A. Bradley, D. Byram et al., *Technical results from the surface run of the LUX dark matter experiment*, *Astropart. Phys.* **45** (2013) 34–43.
- [10] A. Morozov, I. Defendi, R. Engels, F. a. F. Fraga, M. M. F. R. Fraga, A. Gongadze et al., *Adaptive algorithms of position and energy reconstruction in anger-camera type detectors: experimental data processing in ANTS*, 2013 *JINST* **8** P05002.
- [11] A. Morozov, V. Solovov, F. Alves, V. Domingos, R. Martins, F. Neves, and V. Chepel, *Iterative reconstruction of detector response of an Anger gamma camera*, *Phys. Med. Biol.*, **60** (2015) no. 10, 4169.
- [12] J. Joung, R. Miyaoka, S. Kohlmyer, and T. Lewellen, *Implementation of ML based positioning algorithms for scintillation cameras*, *IEEE Trans. on Nuc. Sci.* **47** (2000), no. 3, Part 3 1104–1111.
- [13] M. Unser, *Splines: A Perfect Fit for Signal and Image Processing*, *IEEE Signal Process. Mag.* **16:6** (1999), 22–38.
- [14] F. Brunet, *Contributions to Parametric Image Registration and 3D Surface Reconstruction*, *Ph.D thesis* (2010).
- [15] <http://www.coimbra.lip.pt/ANTS/index.html>
- [16] <http://www.sensl.com/downloads/ds/DS-MicroCseries.pdf>,
<http://www.sensl.com/downloads/ds/UM-ArraySMT.pdf>